Reac Kinet Mech Cat (2014) 111:371–382
DOI 10.1007/s11144-013-0623-9

Preparation of $WO_3/TiO_2/In_2O_3$ composite structures and their enhanced photocatalytic activity under visible light irradiation

Ashok Kumar Chakraborty · Md. Masudur Rhaman · Md. Emran Hossain · K. M. A. Sobahan

Received: 15 January 2013 / Accepted: 8 August 2013 / Published online: 15 August 2013

Abstract A novel visible light ($\lambda \geq 420$ nm) active $WO_3/TiO_2/In_2O_3$ composite photocatalyst was prepared by a two-step process. At first, TiO_2/In_2O_3 was synthesized utilizing maleic acid as an organic linker. Afterwards, $WO_3/TiO_2/In_2O_3$ composite heterojunction structure was prepared by the incipient wetness method. The composite was characterized by SEM mapping, high-resolution TEM, BET, UV–Vis diffuse reflectance spectroscopy, XPS and surface acidity measurement. The photocatalytic activity of the composite was evaluated through the decomposition of organic pollutants in gas and aqueous phases. The $WO_3/TiO_2/In_2O_3$ composite demonstrated greatly improved photocatalytic efficiency in compare with TiO_2/In_2O_3 composite and Degussa P25 for the degradation of gaseous 2-propanol and evolution of CO_2 and, 1,4-terephthalic acid in aqueous phase under visible light ($\lambda \geq 420$ nm) irradiation. The concentration of WO_3 in the composite was optimized to 3.5 mol% $WO_3/TiO_2/In_2O_3$. Based upon these observations, the mechanistic role of WO_3 in enhancing the photocatalytic activity of $WO_3/TiO_2/In_2O_3$ has been suggested.

Keywords Nano heterojunction · Photocatalyst · Visible light · Organic compounds · Environment · CO_2

A. K. Chakraborty (✉) · Md. M. Rhaman · Md. E. Hossain
Department of Applied Chemistry and Chemical Technology, Islamic University, Kushtia 7003, Bangladesh
e-mail: akc_iu@yahoo.co.uk

K. M. A. Sobahan
Department of Applied Physics, Electronics & Communication Engineering, Islamic University, Kushtia 7003, Bangladesh

Introduction

Heterogeneous photocatalysis over either pure phase or multiple metal oxide composite semiconductors is a promising method for the elimination of toxic organic compounds from the environment by their transformation into harmless species under visible light ($\lambda \geq 420$ nm) [1–5]. A variety of semiconductor-based photocatalysts such as TiO_2, ZnO, CdS, ZnS, SnO_2, Ag_3PO_4, $FeTiO_3$, WO_3 and so on and, their composites have been successfully fabricated and photocatalytic properties have been extensively explore [6–16]. These nanocrystalline composite systems demonstrate significantly enhanced photocatalytic performance in the degradation of organic pollutants in air and water, as the composite could facilitate charge transfer and suppress the recombination of electron-hole pairs in the photocatalysts in these systems. However, their relatively low activities in the visible light region due to low adsorption towards organics limit their practical use in air and water purification. Therefore, the exploration of new semiconductor materials with high adsorption affinity as highly efficient visible light induced photocatalysts is of significant importance, and is also a great challenge. The trigger step for the photocatalytic degradation of pollutants is to enhance the adsorption ability of the photocatalyst towards the organic pollutants. The technique of supporting as well as modifying the surface is effective to improve the adsorption abilities of solid photocatalysts. On the one hand, it is envisaged that the improved adsorption ability could enable a reactant-rich environment. Conversely, it would give rise to a strengthened interaction between the reactant molecules and the catalyst surface, which is of particular interest for heterogeneous photocatalytic degradation reaction [17–21]. WO_3 is an influential candidate to cover the solid catalyst surface as well as to increase the adsorption ability of the catalyst due to its acidic nature. In an attempt to prepare a surface modified photocatalysts, we modified the surface of TiO_2 nanoparticles (Degussa P25) and $BiOCl/Bi_2O_3$ composite with WO_3 previously [20, 21]. By the incorporation of WO_3, the catalysts were much less agglomerated and more stably suspended in aqueous solution and the photocatalytic activity in decomposing organic pollutants was greatly improved owing to the dramatic increase in surface acidity as well as adsorption ability. Similar results have also been reported by several other research groups [17–19, 22, 23].

In our previous report [24], it has been shown that the pure In_2O_3/TiO_2 composite is active in decomposing organic pollutants under visible light ($\lambda \geq 420$ nm) irradiation. Even though this system revealed a notable visible light photocatalytic activity, its activity would not be high enough due to poor adsorption behavior of the composite system towards the organic pollutants. Thus, it is expected that WO_3-covered In_2O_3/TiO_2 composite structure will exhibit enhanced photocatalytic efficiency towards the organic compounds.

In this study, for the first time, we have modified In_2O_3/TiO_2 composite photocatalysts with WO_3 by a simple incipient wetness method and demonstrated the photocatalytic behavior in decomposing organic pollutants in gas and solution phases under visible light irradiation ($\lambda \geq 420$ nm). We envisage that this study could provide new insights and better understanding on the mechanism of

photocatalytic enhancement for the WO_3 modified In_2O_3/TiO_2 composite photocatalyst.

Experimental

The preparation method of 7/93 TiO_2/In_2O_3 composite (the composite consisting of 7 % In_2O_3 and 93 % TiO_2) utilized in this experiment was based on our previous report [24]. In brief, 0.1129 g of In_2O_3 (Aldrich, 99.99 %, particle size, 100–600 nm) was added into 40 mL absolute ethanol to give a suspension with a subsequent addition of 0.1887 g maleic acid. 1.5 g of TiO_2 nanoparticles (Degussa P25) was then added in the reaction mixture while stirring vigorously for 6 h at room temperature. Afterwards, the resultant composite materials were precipitated by centrifugation. The collected mixture was then washed several times with ethanol and was dried at 60 °C for 12 h. Finally, the dried powder was annealed at 300 °C for 2 h to form the desired composite product.

$WO_3/TiO_2/In_2O_3$ composite photocatalysts were prepared by incipient wetness method. In a typical experiment, for 3.5 mol% $WO_3/TiO_2/In_2O_3$, 1.5 g of TiO_2/In_2O_3 composite was suspended in ammonia solution dissolved with 0.1450 g of H_2WO_4 (Aldrich), and dried in a water bath with stirring at 65 °C. The samples were then heat-treated at 230 °C for 2 h.

During the photocatalytic measurements, the photocatalysts samples were irradiated under 300 W xenon lamp for 3 h in a film form to remove any possible organic residuals. The photocatalytic efficiency of $WO_3/TiO_2/In_2O_3$ was measured in gas phase using 2-propanol (IP) as a model compound. Aqueous colloidal suspensions containing 50 μmol of catalysts were spread as a film on a 2.5 × 2.5 cm^2 Pyrex glass, and subsequently dried at room temperature overnight. The dried films were used for the photocatalytic reaction without further heat treatment. The gas reactor system used for this photocatalytic reaction is described elsewhere [19]. The net volume of the gas tight reactor was 200 mL, and the catalyst film was located at the center of the reactor. The whole area of catalyst film (2.5 cm × 2.5 cm) was irradiated by a 300 W xenon lamp through an UV cut-off filter ($\lambda < 420$ nm, Oriel) and a water filter to cut off infrared. After the evacuation of the reactor, 0.08 mL of IP mixed in 1.6 mL of water was injected into the reactor. Then the initial concentration of gaseous IP in the reactor was kept to 117 ppm in volume (ppmv). Thus, the ultimate concentration of CO_2 evolved will be 351 ppmv when the whole amount of IP is completely decomposed, as shown in the following equation.

$$2(CH_3)_2CHOH(g) + 9O_2 \rightarrow 6CO_2(g) + 8H_2O(g)$$

The total pressure of the reactor was then controlled to 750 Torr by the addition of oxygen gas. Under these conditions, IP and H_2O remained in the vapor phase. After a certain time of irradiation, 0.5 mL of the gas in the reactor was automatically picked up and sent to a gas chromatograph (Agilent Technologies, Model 6890 N) by using an auto sampling valve system. For the detection of CO_2, a methanizer was installed between the GC column outlet and the FID detector.

To evaluate the photocatalytic efficiency of the catalyst in aqueous phase, 1,4-terephthalic acid (TPA) was utilized as a model compound. 50 μmol of catalyst was suspended in 50 mL (0.0986 g/L) of 1×10^{-4} M TPA aqueous solution. Samples were then irradiated by a 300 W xenon lamp through an UV cut-off filter ($\lambda < 420$ nm, Oriel) and a water filter to cut off infrared. After every 30 min of irradiation, the concentration of remaining organic pollutants in the solution was measured with a UV–Vis spectrophotometer (Perkin-Elmer Lambda 40).

The Lewis surface acidity was evaluated by titrating 1.0 g of photocatalyst samples suspended in benzene with 10.0 mL of 0.1 N *n*-butylamine benzene solution, using methyl red as indicator [20, 22, 25]. X-ray powder diffraction patterns for the $WO_3/TiO_2/In_2O_3$ particles were obtained by using a Rigaku Multiflex diffractometer. Philips CM30 transmission electron microscope operated at 250 kV was used for the TEM images of $WO_3/TiO_2/In_2O3$ particles. SEM images of TiO_2 samples were observed by a field emission scanning electron microscope (FE-SEM, Hitachi S-4500). X-ray photoelectron spectroscopy (XPS) [Sigma Probe Instrument (Thermo VG, UK)] analyses of the samples were carried out in an ultrahigh vacuum (UHV) chamber with a base pressure below 5×10^{-9} Torr at room temperature. It was equipped with a standard monochromatic Al K_α excitation source ($hv = 1486.6$ eV). The binding energy (BE) was referenced to the C 1s peak at 284.6 eV. The UV–Vis diffuse reflectance spectra were achieved using a Perkin-Elmer Lambda 40.

Results and discussion

Scheme 1 shows the plausible mechanism of the formation of $WO_3/TiO_2/In_2O_3$ core-shell like heterojunction structure. The large In_2O_3 particles were covered with 25–30 nm sized TiO_2 nanoparticles and made a tight intimate contact by maleic acid. Afterwards, the maleic acid was eliminated during heat treatment at 300 °C for 2 h as we reported previously. 7/93 TiO_2/In_2O_3 demonstrated the optimized photocatalytic efficiency in decomposing organic compounds in gas phase as well as aqueous phase. Here, 7/93 TiO_2/In_2O_3 composite was utilized to modify the surface with various amount of tungsten oxide for further enhancement of photocatalytic efficiency under visible light. Thus, in the $WO_3/TiO_2/In_2O_3$ core-shell like structure, WO_3 exists on the surface and adsorbs the organic molecules.

X-ray diffraction (XRD) was applied to investigate the phase structures of WO_3 anchored TiO_2/In_2O_3 composite powders. Fig. 1 shows the XRD patterns of the

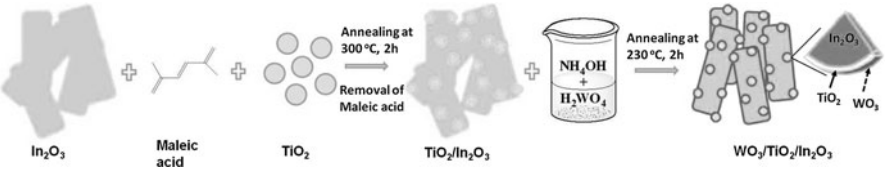

Scheme 1 Schematic representation of the preparation of $WO_3/TiO_2/In_2O_3$ composite photocatalyst

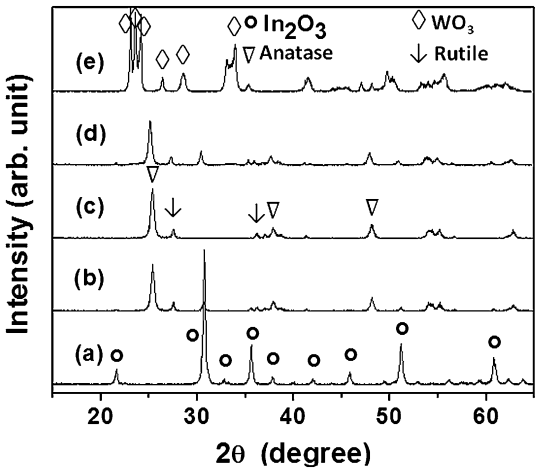

Fig. 1 XRD patterns of **a** In_2O_3, **b** TiO_2/In_2O_3 composite, **c** TiO_2, **d** 3.5 mol% $WO_3/TiO_2/In_2O_3$ composite and **e** WO_3 photocatalysts

TiO_2 nanopowder, In_2O_3, TiO_2/In_2O_3 composite, WO_3 and as prepared 3.5 mol% $WO_3/TiO_2/In_2O_3$ composite photocatalyst obtained from TiO_2/In_2O_3 composite. XRD analysis of the samples showed that pure In_2O_3 (Fig. 1a), TiO_2 (Fig. 1c) and WO_3 (Fig. 1e) powders were well crystallized. They can well be indexed to In_2O_3 (JCPDF # 71-2195), Degussa P25 and WO_3 (JCPDF #20-1323). Fig. 1b presents the phase structure of the 7/93 TiO_2/In_2O_3 composite. No obvious diffraction peaks due to WO_3 was not observed in 3.5 mol% $WO_3/TiO_2/In_2O_3$ composite as shown in Fig. 1d, since the composite was annealed at 230 °C for 2 h. This annealing temperature was not high enough for the formation of highly crystallized WO_3 phase. Thus, WO_3 exists in $WO_3/TiO_2/In_2O_3$ composite as an amorphous state.

A SEM image of the 3.5 mol% $WO_3/TiO_2/In_2O_3$ composite photocatalyst and its corresponding elemental mapping (tungsten) image are shown in Fig. 2. It is clear from the Fig. 2 that the morphologies are quite similar in both images (Fig. 2a, b). The tungsten (W) mapping as shown in Fig. 2b indicates that tungsten is uniformly dispersed over the entire surface of the TiO_2/In_2O_3 composite.

The high resolution TEM images shown in Fig. 3 indicates that comparatively larger In_2O_3 particles are completely covered with 25–30 nm sized TiO_2 nanoparticles (Degussa P25). The uniform lattice fringes were observed over the entire surface of TiO_2/In_2O_3 heterojunction as shown in Fig. 3a. Similar lattice fringes were observed for 3.5 mol% $WO_3/TiO_2/In_2O_3$ composite. However there were no cluster structures of the tungsten oxide were found around the $WO_3/TiO_2/In_2O_3$ composite as indicated in Fig. 3b. This suggests that the tungsten oxide was highly dispersed on the surface of the TiO_2/In_2O_3 composite.

UV–Vis spectral measurements were employed to measure the changes in the reflectance edge of the TiO_2, In_2O_3, TiO_2/In_2O_3 composite, 3.5 mol% $WO_3/TiO_2/In_2O_3$ and WO_3 as shown in Fig. 4. These indicate that bare In_2O_3 and TiO_2 could absorb solar energy with a wavelength shorter than 560 and 385 nm, respectively. The reflectance edge of 3.5 mol% $WO_3/TiO_2/In_2O_3$ is comparable with TiO_2/In_2O_3 composite photocatalyst, suggesting that the band edge of TiO_2/In_2O_3 composite was not significantly altered by the loading of WO_3. Moreover, the dispersed WO_3

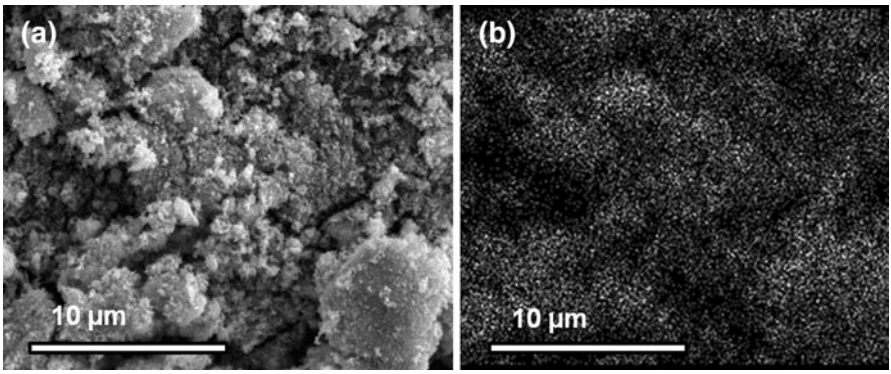

Fig. 2 SEM image of **a** 3.5 mol% $WO_3/TiO_2/In_2O_3$ composite and **b** its corresponding tungsten (W) mapping

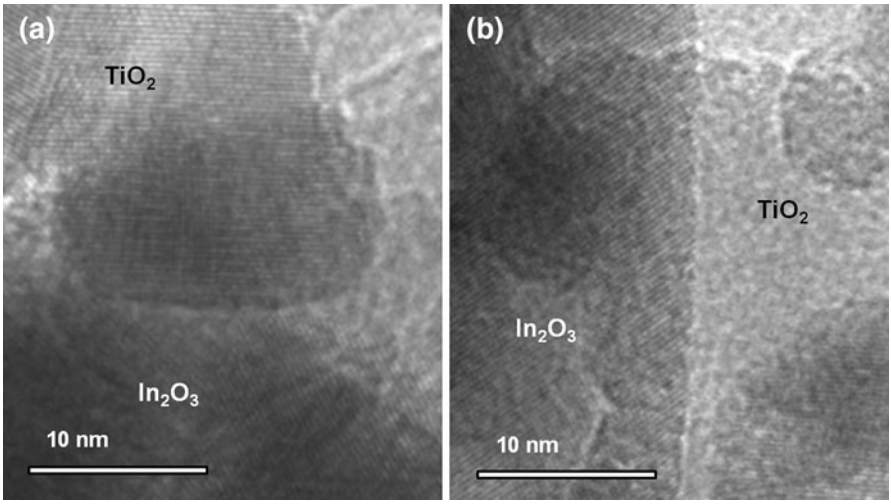

Fig. 3 High-resolution TEM images of **a** TiO_2/In_2O_3 and **b** 3.5 mol% $WO_3/TiO_2/In_2O_3$ composite photocatalysts

was in amorphous phase as indicated in Fig. 1d. Thus, the loading of WO_3 onto the heterojunction of TiO_2/In_2O_3 composite does not modify the band structure of TiO_2/In_2O_3 composite photocatalyst.

In order to analyze the chemical composition and oxidation state of the composite, XPS spectra of 3.5mol% $WO_3/TiO_2/In_2O_3$ composite photocatalyst calcined at 230 °C were considered. Fig. 5 shows the high resolution XPS survey scan of O 1s and W 4f which were taken on the surface of composite. The O 1s peak, as shown in Fig. 5a, was considerably broader and thus deconvoluted into two peaks. The peaks centered at 530.03 eV should be assigned to O 1s region of Ti–O and In–O, whereas the peak at 531.59 eV assigned to the surface hydroxyl groups. The presence of the peak at 531.59 eV clearly indicates that the $WO_3/TiO_2/In_2O_3$

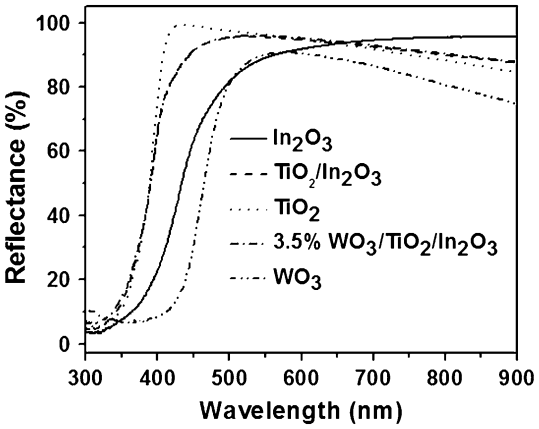

Fig. 4 UV-Vis diffuse reflectance spectra of In_2O_3, TiO_2/In_2O_3 composite, TiO_2, 3.5 mol% $WO_3/TiO_2/In_2O_3$ composite and WO_3 photocatalysts

composite photocatalyst contains surface hydroxyl groups as well as water. The $WO_3/TiO_2/In_2O_3$ composite has higher adsorption affinity. From the high resolution XPS of W 4f as shown in Fig. 5b, the peaks having the binding energy 35.84 and 38.02 eV are corresponding to W $4f_{7/2}$ and W $4f_{5/2}$, respectively, which are the typical binding energies of W^{6+}. This suggests that the incorporated W species in $WO_3/TiO_2/In_2O_3$ was WO_3 [20, 26].

The photocatalytic activities of $WO_3/TiO_2/In_2O_3$ samples were measured on the degradation of IP in gas phase under visible light ($\lambda \geq 420$ nm) irradiation and represented in Fig. 6. Photocatalytic decomposition of IP was plotted as ln[c] versus irradiation time. The photodegradation followed first order kinetics, which can be expressed as follows: $-d[c]/dt = k_r[c]$, where [c] is the concentration of gaseous IP, k_r is the overall rate constant and t is the reaction time. Here, k_r was defined as photocatalytic activity. As a comparison, the photocatalytic activity of TiO_2/In_2O_3 composite, TiO_2 nanoparticles, In_2O_3, WO_3 was included in Fig. 6a. TiO_2

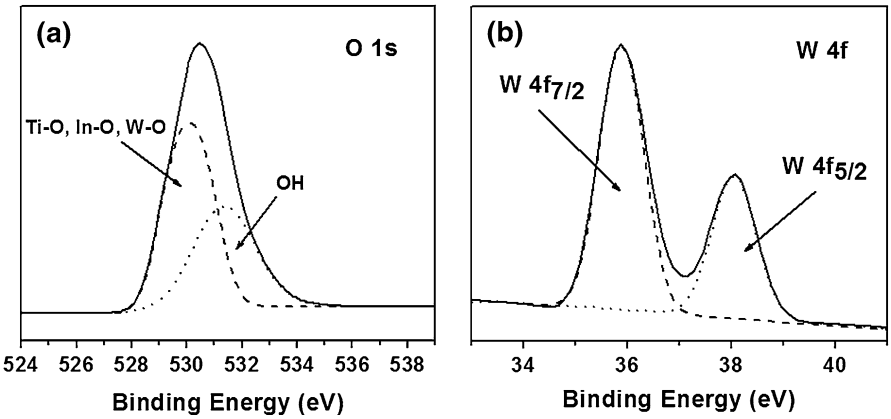

Fig. 5 High resolution XPS spectrum of 3.5 mol% $WO_3/TiO_2/In_2O_3$ composite photocatalyst **a** O 1s and **b** W 4f

nanoparticles, In_2O_3, WO_3 show no apparent photocatalytic activity under visible light irradiation. $WO_3/TiO_2/In_2O_3$ composites with a wide range of WO_3 content demonstrate a high level of activity for the degradation of IP under visible light. The photocatalytic activity was optimized to 3.5 mol% $WO_3/TiO_2/In_2O_3$ and a further increase of WO_3 over 3.5 mol% rapidly decreased its efficiency. However, in comparison with the 3.5 mol% $WO_3/TiO_2/In_2O_3$ composite, poor activity was obtained on the TiO_2/In_2O_3 composite under the same experimental condition. Under these conditions, the 3.5 mol% $WO_3/TiO_2/In_2O_3$ composite presented 2.1 and 13.7 times higher photocatalytic activity than that of TiO_2/In_2O_3 composite and TiO_2 (Degussa P25), respectively. A similar trend was observed in evolving CO_2, as illustrated in Fig. 6b. It was found that the CO_2 evolved in 120 min of visible irradiation with 3.5 mol% $WO_3/TiO_2/In_2O_3$ was 2.5 times greater than that of TiO_2/In_2O_3. Similarly, it was 12 times higher than that with the TiO_2 nanoparticles (Degussa P25).

We also evaluated photocatalytic activities of $WO_3/TiO_2/In_2O_3$ for the degradation of TPA in aqueous phase under visible light ($\lambda \geq 420$ nm) and compared their activities with TiO_2/In_2O_3, TiO_2, In_2O_3 and WO_3. It was found that $WO_3/TiO_2/In_2O_3$ in several compositions of WO_3 was also active to degrade TPA under visible light (Fig. 6c). The degradation efficiency of 3.5 mol% $WO_3/TiO_2/In_2O_3$ was higher among the compositions of WO_3 and pure TiO_2/In_2O_3 composite and, much higher than that of P25. The photocatalytic efficiency with 3.5 mol% $WO_3/TiO_2/In_2O_3$ was 2.2 times than that of TiO_2/In_2O_3 and it was 21.1 times in comparison with TiO_2 nanoparticles (Degussa P25) in 120 min under visible light irradiation. Therefore, $WO_3/TiO_2/In_2O_3$ materials are promising photocatalysts under visible light irradiation, while 3.5 mol% $WO_3/TiO_2/In_2O_3$ exhibited the best photocatalytic activity among the composites. The higher photocatalytic activity of WO_3 loaded TiO_2/In_2O_3 is attributed to its higher adsorption ability towards the organics. The detailed results of the photocatalytic catalytic experiments in gas as well as in aqueous phases are given in Table 1.

The surface acidity of $WO_3/TiO_2/In_2O_3$ as a function of WO_3 is shown in Fig. 7. The surface acidity of the resultant $WO_3/TiO_2/In_2O_3$ composite photocatalyst was appreciably increased by the introduction of WO_3, since WO_3 is highly acidic in nature. The increment of acidity was very high by the initial addition of WO_3. That is, by the introduction of 1 mol% WO_3, the surface acidity went up from 0.04 to 0.13 mmol g^{-1}. However, the surface acidity was not significantly changed with higher content of WO_3 over 3.5 mol%. Fig. 7 illustrates the trend of photocatalytic efficiency of $WO_3/TiO_2/In_2O_3$ as a function of WO_3 composition. The photocatalytic activity for the decomposition of IP in gas phase was optimized in the range of 3–5 mol% of WO_3. It is expected that WO_3 preferentially binds to the surface of the TiO_2/In_2O_3 composite with a high binding affinity between the WO_3 and the composite. Thus, most of the WO_3 remains in a highly dispersed molecular species on the surface of the composite. For higher concentrations of WO_3, the excess WO_3 will be segregated by itself or multilayers will be formed. This is clearly supported by the surface acidity measurement, since the surface acidity was not significantly changed over 3.5 mol% of WO_3 as shown in Fig. 7.

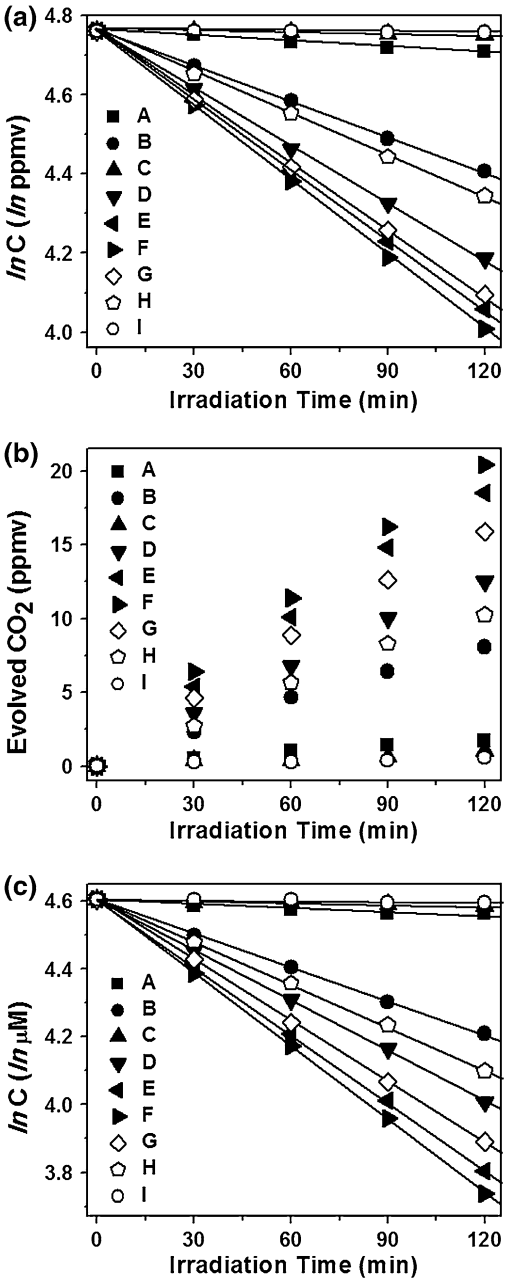

Fig. 6 Activities of TiO_2 nanoparticles (Degussa P25), TiO_2/In_2O_3 composite, In_2O_3, WO_3 and $WO_3/TiO_2/In_2O_3$ composite photocatalysts on the photodegradation of **a** gaseous 2-propanol (IP), **b** evolution CO_2 and **c** decomposition of aqueous 1,4-terephthalic acid (TPA) under visible light ($\lambda \geq 420$) irradiation. *A* TiO_2 (Degussa P25); *B* TiO_2/In_2O_3; *C* In_2O_3; *D* 2.5 mol% $WO_3/TiO_2/In_2O_3$; *E* 3.0 mol% $WO_3/TiO_2/In_2O_3$; *F* 3.5 mol% $WO_3/TiO_2/In_2O_3$; *G* 4.0 mol% $WO_3/TiO_2/In_2O_3$; *H* 4.5 mol% $WO_3/TiO_2/In_2O_3$; *I* WO_3

Table 1 BET surface area of various catalysts and photocatalytic degradation of gaseous 2-propanol (IP) and aqueous 1,4-terephthalic acid (TPA) for 120 min under visible light ($\lambda \geq 420$ nm)

Photocatalyst samples	BET surface area (m^2/g)	Degradation of gaseous IP				Specific photocatalytic activity (min^{-1} m^{-2})	Degradation of 1,4-terephthalic acid (TPA)		Specific photocatalytic activity (min^{-1} m^{-2})
		Adsorbed amount of IP (%)	IP degraded, [ln c]	Rate constant, k (min^{-1})	Evolved CO_2 (ppmv)		TPA degraded, [ln c]	Rate constant, k (min^{-1})	
TiO_2	50	5.7	4.70953	4.62×10^{-4}	1.7	0.00231	4.56435	3.41×10^{-4}	0.00170
TiO_2/In_2O_3	47	4.9	4.40672	2.98×10^{-3}	8.1	0.01353	4.20916	3.30×10^{-3}	0.01498
In_2O_3	2.5	2.3	4.75186	9.73×10^{-5}	1.0	0.00280	4.58497	1.52×10^{-4}	0.00438
2.5 mol% $WO_3/TiO_2/In_2O_3$	48	8.2	4.18525	4.81×10^{-3}	12.5	0.02062	4.00733	4.96×10^{-3}	0.02126
3.0 mol% $WO_3/TiO_2/In_2O_3$	48	11.3	4.05751	5.88×10^{-3}	18.5	0.02503	3.80425	6.68×10^{-3}	0.02844
3.5 mol% $WO_3/TiO_2/In_2O_3$	49	12.5	4.00733	6.32×10^{-3}	20.4	0.02617	3.73767	7.20×10^{-3}	0.02981
4 mol% $WO_3/TiO_2/In_2O_3$	49	13.6	4.09434	5.56×10^{-3}	15.9	0.02286	3.88997	5.97×10^{-3}	0.02455
4.5 mol% $WO_3/TiO_2/In_2O_3$	49	14.1	4.34381	3.49×10^{-3}	10.3	0.01425	4.09911	4.19×10^{-3}	0.01711
WO_3	0.84	16.4	4.75789	4.28×10^{-5}	0.6	0.00440	4.59512	1.00×10^{-4}	0.01027

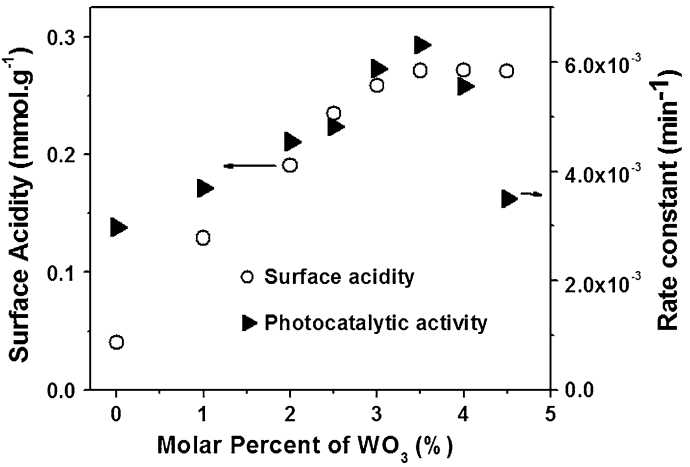

Fig. 7 Surface acidity and photocatalytic degradation rate constants of $WO_3/TiO_2/In_2O_3$ composite photocatalyts as a function of WO_3

With the accumulation of WO_3, the change of BET surface area of $WO_3/TiO_2/In_2O_3$ composite was not significant. The surface area of the TiO_2/In_2O_3 composite was 47 m^2/g whereas for the 3.5 mol% $WO_3/TiO_2/In_2O_3$ composite was 49 m^2/g as shown in Table 1. Thus, the enhancement of photocatalytic activity of $WO_3/TiO_2/In_2O_3$ composite was not caused by the increase in surface area. We believe that the enhancement is due to increase in surface acidity with the incorporation of WO_3.

In the present study, the heterojunction structure of pure TiO_2/In_2O_3 exhibited a lower photocatalytic activity, but after loading of WO_3 onto TiO_2/In_2O_3 composite, $WO_3/TiO_2/In_2O_3$ demonstrated notably high photocatalytic efficiency under a visible light irradiation. The heterogeneous photocatalytic reactions between solid, liquid and/or gas take place on the solid surface. Thus, the adsorption of pollutants onto the photocatalyst surface would be the important factor. It is indicated that, WO_3 retains a much higher Lewis surface acidity than TiO_2 and In_2O_3. It was found that by loading 3.5 mol% WO_3 onto TiO_2/In_2O_3 composite, it makes a homogeneous monolayer on the surface of TiO_2/In_2O_3 composite. Hence, the Lewis surface acidity was highly increased as indicated in Fig. 7. Therefore, WO_3 has a higher affinity for chemical species having unpaired electrons. Hence, $WO_3/TiO_2/In_2O_3$ heterojunction photocataysts can adsorb a greater amount of OH^- or H_2O, which are prerequisite for the generation of OH radicals. Consequently, WO_3 films strongly adsorb and gather more organic pollutants onto the surface of $WO_3/TiO_2/In_2O_3$ composite, which may enhance the interaction between organic molecules and composite photocatalysts on the WO_3 films. The high adsorption abilities of the $WO_3/TiO_2/In_2O_3$ catalyst surface towards organic pollutant would enhance the electron/hole transfer efficiency and contact opportunity with photogenerated active species. The high photocatalytic activity towards our composite system might be due to the adsorption ability of $WO_3/TiO_2/In_2O_3$ to organics.

Conclusion

Novel visible light ($\lambda \geq 420$ nm) induced $WO_3/TiO_2/In_2O_3$ composite photocatalysts were prepared by introducing WO_3 onto the TiO_2/In_2O_3 composite. WO_3 was well dispersed on the composite surface. The surface acidity of the composite was maximized at 3.5 mol% $WO_3/TiO_2/In_2O_3$. At this composition, the heterojunction demonstrated strong adsorption behavior towards the organic compounds compared to the case with TiO_2/In_2O_3 heterojunction, due to its high Lewis acidity on the surface and had obviously enhanced the photocatalytic activity in IP degradation in the gas phase and evolution of CO_2 and, decomposition of TPA in aqueous phase among the $WO_3/TiO_2/In_2O_3$ composites, TiO_2/In_2O_3 heterojunction and TiO_2 nanoparticles (Degussa P25). Thus, the novel heterojunction materials, as highly efficient photocatalysts, may have potential applications in the removal of pollutants from air and water.

References

1. Fujishima A, Honda K (1972) Nature 238:37–38
2. Kubacka A, Fernández-García M, Colón G (2012) Chem Rev 112:1555–1614
3. Chen X, Mao SS (2007) Chem Rev 107:2891–2959
4. Asahi R, Morikawa T, Ohwaki T, Aoki K, Taga Y (2001) Science 293:269–271
5. Nakata K, Ochiai T, Murakami T, Fujishima A (2012) Electrochim Acta 84:103–111
6. Rawal SB, Chakraborty AK, Kim YJ, Kim HJ, Lee WI (2012) RSC Advances 2:622–630
7. Kim YJ, Gao B, Han SY, Jung MH, Chakraborty AK, Ko T, Lee C, Lee WI (2009) J Phys Chem C 113:19179–19184
8. Zhang Z, Wang W, Wang L, Sun S (2012) ACS Appl Mater Interf 4(2):593–597
9. Kim HL, Moon GH, Monllor-Satoca D, Park Y, Choi W (2012) J Phys Chem C 116:1535–1543
10. Nakata K, Fujishima A (2012) J Photochem Photobiol A 13:169–189
11. Kanmoni VGG, Daniel S, Raj GAG (2012) Reac Kinet Mech Cat 106:325–339
12. Xiang Q, Yu J, Jaroniec M (2012) J Am Chem Soc 134:6575–6578
13. Bojinova A, Dushkin C (2011) Reac Kinet Mech Cat 103:239–250
14. Wang P, Huang B, Qin X, Zhang X, Dai Y, Wei J, Whangbo M (2008) Angew Chem 120:8049–8051
15. Chakraborty AK, Kebede MA (2012) Reac Kinet Mech Cat 106:83–98
16. Wang H, Gao J, Guo TQ, Wang RM, Guo L, Liu Y, Li JH (2012) Chem Commun 48:275–277
17. Liu L, Liu J, Sun DD (2012) Catal Sci Technol 2:2525–2532
18. Xiong ZG, Zhang LL, Ma JZ, Zhao XS (2010) Chem Commun 46:6099–6101
19. Kwon YT, Song KY, Lee WI, Choi GJ, Do YR (2000) J Catal 191:192–199
20. Chakraborty AK, Rawal SB, Han SY, Chai SY, Lee WI (2011) Appl Catal A 407:217–223
21. Chakraborty AK, Chai SY, Lee WI (2008) Bull Korean Chem Soc 29:494–496
22. Pan JH, Lee WI (2006) Chem Mater 18:847–853
23. Keller V, Bernhardt P, Garin F (2003) J Catal 215:129–138
24. Chakraborty AK, Kebede MA (2012) J Clust Sci 23:247–257
25. Song KY, Park MK, Kwon YT, Lee HW, Chung WJ, Lee WI (2001) Chem Mater 13:2349–2355
26. Wagner CD, Riggs WM, Davis LE, Moulder JF (1979) Handbook of X-ray photoelectron spectroscopy. Perkin-Elmer Corporation, Waltham